

The impact of the diurnal cycle on the MJO over the Maritime Continent: a modeling study assimilating TRMM rain rate into global analysis

Ji-Hyun Oh · Baek-Min Kim · Kwang-Yul Kim ·
Hyo-Jong Song · Gyu-Ho Lim

Received: 14 November 2011 / Accepted: 4 June 2012 / Published online: 19 June 2012
© Springer-Verlag 2012

Abstract In the present study, we use modeling experiments to investigate the impact of the diurnal cycle on the Madden-Julian Oscillation (MJO) during the Australian summer. Physical initialization and a nudging technique enable us to assimilate the observed Tropical Rainfall Measuring Mission (TRMM) rain rate and atmospheric variables from the National Centers for Environmental Prediction—National Center for Atmospheric Research Reanalysis 2 (R2) into the Florida State University Global Spectral Model (FSUGSM), resulting in a realistic simulation of the MJO. Model precipitation is also significantly improved by TRMM rain rate observation via the physical initialization. We assess the influence of the diurnal cycle on the MJO by modifying the diurnal component during the model integration. Model variables are nudged toward the daily averaged values from R2. Globally suppressing the diurnal cycle (NO_DIURNAL) exerts a strong impact on the Maritime Continent. The mean state of precipitation increases and intraseasonal variability becomes stronger over the region. It is well known that MJO weakens as it passes over the Maritime Continent. However, the MJO maintains its strength in the NO_DIURNAL experiment,

and the diminution of diurnal signals during the integration does not change the propagating speed of the MJO. We suggest that diminishing the diurnal cycle in NO_DIURNAL consumes less moist static energy (MSE), which is required to trigger both diurnal and intraseasonal convection. Thus, the remaining MSE may play a major role along with larger convective instability and stronger lower level moisture convergence in intensifying the MJO over the Maritime Continent in the model simulation.

1 Introduction

The Madden-Julian Oscillation (MJO) is a dominant physical mode of the tropical intraseasonal variability (Madden and Julian 1994). The MJO exhibits the characteristics of a Kelvin-Rossby wave packet associated with deep convection (Gill 1980). It is quasi-periodic, ranging from 30 to 60 days, and is characterized by the eastward propagation of enhanced and suppressed convection, mainly over the Indian Ocean, the west Pacific Ocean, and the Maritime Continent. The Maritime Continent, which comprises a complex system of islands and adjacent seas, is known to be a major atmospheric heat source that plays an essential role in the global climate system (Neale and Slingo 2003; Ichikawa and Yasunari 2006). Geographical and thermodynamic conditions in the region are favorable for the development of deep convection on multiple temporal and spatial scales throughout the year. Since the Maritime Continent separates the Pacific and Indian Oceans, the free mixture of water ceases and warm water is accumulated, presumably because of easterly winds on the eastern side of New Guinea (Cane and Molnar 2001; Rodgers et al. 2000). The islands also act as a heat source for the overlying atmosphere by providing sensible heating,

J.-H. Oh · K.-Y. Kim · G.-H. Lim (✉)
School of Earth and Environmental Sciences,
Seoul National University, Seoul, Korea
e-mail: gyuholim@snu.ac.kr

J.-H. Oh
Center for Ocean-Atmospheric Prediction Studies,
The Florida State University, Tallahassee, FL, USA

B.-M. Kim
Korea Polar Research Institute, KORDI, Incheon, Korea

H.-J. Song
Korea Institute of Atmospheric Prediction Systems, Seoul, Korea

which triggers the ascent of air. If the ascending air is moist, latent heat is released when the moist air rises high enough to condense (Dayem et al. 2007). In particular, there is a distinct land–sea contrast in the diurnal variation over the Maritime Continent. The land–sea breezes caused by the local temperature and pressure gradients are known to be closely related to the differences in rainfall amounts between the land and the sea (Qian 2008; Oh et al. 2012). The diurnal cycle in the tropics is a principal mode of variability in the global climate system (Yang and Slingo 2001), and its characteristics and mechanisms have been studied extensively (Chen and Houze 1997; Sui et al. 1997; Lim and Suh 2000; Ichikawa and Yasunari 2006). Though the diurnal variations of tropical deep convection largely depend on the region, it is generally accepted that the convective or precipitation maximum occurs over the continents in the late afternoon or early evening and over the ocean in the early morning (Sui et al. 1997; Yang and Slingo 2001; Bowman et al. 2005).

The MJO tends to be weakened as it passes over the Maritime Continent and then is rejuvenated as the convection moves out into the west Pacific (Rui and Wang 1990; Salby and Hendon 1994; Seo and Kim 2003; Inness and Slingo 2006; Kim et al. 2009). Inness and Slingo (2006) described possible mechanisms associated with the weakening of the MJO as it crosses the Maritime Continent. In summary, they found the island landmasses disturb the air–sea interaction and low-level wind anomalies that are essential for the development of the MJO. However, they determined that the orographic blocking effect of the islands, rather than the presence of the islands alone, is the most likely contributor to the weakening of the MJO. Wu and Hsu (2009) also demonstrated flow bifurcation around the elongated mountainous islands when the MJO reaches the Maritime Continent. In addition, the existence of topography tends to create extra lifting and sinking within the large-scale circulation, thus the convective systems are observed to diminish or generate on different sides of the tropical topography.

Taking different approach, Inness and Slingo (2006) discussed scale interaction between the diurnal cycle of convection and the MJO over the Maritime Continent. The scale interaction denotes the two-way process in which the large-scale and low-frequency variability influences the small-scale and high-frequency variability of the climate system and vice versa (Slingo et al. 2003). They hypothesized that the enhanced diurnal cycle of convection around the Maritime Continent affects the development of the MJO by dissipating moist static energy on a short time scale, resulting in the interference of the slow buildup and release of energy associated with the MJO.

According to Lee et al. (2007), the diurnal variation in the moist static energy (MSE) profile shows different characteristics over the land than over the ocean. They

found the diurnal cycle of MSE over land shows daytime development of the atmospheric boundary layer up to the 800-hPa level. At higher levels above the boundary layer, radiative cooling and heating of the atmosphere during the day are dominant. On the other hand, the middle and upper level variability of MSE seems to be important over the ocean. Not only the diurnal cycle but also the MJO is related to MSE in terms of its maintaining mechanism, the recharge-discharge theory. The physical mechanism underlying the MJO remains controversial; nonetheless, the recharge-discharge paradigm emphasizes that a buildup of column MSE occurs before MJO deep convection, and MSE is discharged during and after MJO convection (Bladé and Hartmann 1993; Kemball-Cook and Weare 2001). Accordingly, the MSE is necessary to drive both the diurnal cycle and the MJO.

Although the importance of scale interactions between diurnal, intraseasonal, and seasonal time scales for the mean state and variability of the climate system has been emphasized (Slingo et al. 2003; Qian 2008), relatively less attention has been paid to the scale interaction of the convective system over the Maritime Continent. Understanding the role of multi-scale interactions in regional climate is crucial for climate prediction and for preparing systems to cope with the risks related to the weather and climate.

Using Tropical Rainfall Measuring Mission (TRMM) data, Ichikawa and Yasunari (2006, 2008) showed that the diurnal cycles of rainfall over Borneo and New Guinea, major islands of the Maritime Continent, are modulated by low-level winds varying on intraseasonal time scales. Tian et al. (2006) demonstrated that the amplitude of the diurnal cycle of tropical deep convective cloud (DCC) amount is enhanced (reduced) over both the land and the ocean during the convectively enhanced (suppressed) phase of the MJO whereas the diurnal phase of the DCC is rarely changed by the MJO. Rauniyar and Walsh (2011) investigated the characteristics of the diurnal cycle of rainfall during different phases of the MJO over the Maritime Continent. They showed that the diurnal cycle depends on the phase of the MJO, particularly over the oceanic regions. However, most of the studies on the scale interaction between the diurnal cycle and the MJO have focused on the modulation of the diurnal cycle by the MJO rather than on the influence of the diurnal cycle on the MJO.

In this study, we evaluate the performance of the Florida State University Global Spectral Model (FSUGSM) with respect to the simulation of the MJO, and investigate the influence of the diurnal cycle on the MJO by adopting applied assimilation techniques. We diminish the diurnal cycle in the model simulation by applying the assimilation technique as described in Sect. 2. In Sect. 3, assessment of the performance with respect to the basic climate and intraseasonal oscillation is discussed and climatological

characteristics and the impact of the diurnal cycle on the MJO are examined. We show that even small systematic changes in the diurnal cycle can modify the activity of the MJO over the Maritime Continent through the analysis of model experiments. A plausible explanation is also proposed for the influence of the diurnal cycle on the MJO. A summary and discussion are presented in Sect. 4.

2 Data, model experiments, and methods

2.1 Data

TRMM 3B42 (version 6) rainfall data, which are derived from a combination of high-quality microwave estimates and variable rain rate infrared (IR) estimates, are used for the present study (<http://trmm.gsfc.nasa.gov/3b42.html>). The data are intended to be used to take advantage of the fine scales to create averages appropriate to the user's application (Huffman et al. 1997). The TRMM Multisatellite precipitation Analysis (TMPA) is derived by using an optimal combination of TRMM and other passive microwave precipitation estimates from instruments on-board different low-Earth-orbit satellites. The merged microwave product is calibrated with infrared (IR) estimates from the rapid time capability of geostationary-Earth-orbit satellites as complementary estimates to those from the microwave measurements. The IR radiometer has the advantage of providing estimates with high spatial resolution and very good time sampling. However, the IR radiometer measures the brightness temperature at the top of the cloud, which is an indirect rainfall measuring method. In this regard, rain gauge analyses are also adopted for better estimates (Huffman et al. 1997). Acquired via anonymous ftp from disc2.nascom.nasa.gov, the dataset covers 50°S to 50°N with a 0.25° longitude–latitude spatial resolution at a 3-h time interval. The bi-linearly interpolated dataset to the Gaussian grid of T60 resolution is applied to the assimilation of rain rate for this study.

The National Centers for Environmental Prediction–National Center for Atmospheric Research Reanalysis 2 (NCEP–NCAR R2, hereafter NCEP R2) data, provided by NOAA/OAR/ESRL PSD at their website, are used. We adopt wind, temperature, humidity, and surface pressure from the dataset for the analysis nudging and model initialization. To verify the quality of precipitation simulated by each modeling experiment, daily precipitation from the GPCP 1-degree Daily dataset (GPCP 1DD; GPCP) is employed (Huffman et al. 1997).

2.2 Model experiments

The FSUGSM, which is an atmospheric general circulation model with 27 sigma vertical levels and a horizontal

resolution of T63, is used. Detailed model configuration and selected FSU physics package in this study are described by Cocke and Larow (2000). Using the FSUGSM as a basic modeling system, we adopt the continuous assimilation system by implementing analysis nudging for the model dynamic equation set and a rain rate nudging procedure for the convective parameterization component (in this study, modified Kuo scheme; see Krishnamurti et al. 1983 for details) of the model. The procedure for assimilation of rain rate is based on the method described by Nunes and Cocke (2004). The assimilation technique we use relies largely on a physical initialization (PI) method (Krishnamurti et al. 1991, 1994) that primarily includes rain rate nudging toward observed rain rates as well as Newtonian nudging of prognostic model variables (horizontal winds, temperature, specific humidity, and surface pressure) toward reanalysis. The Newtonian nudging, which keeps the model variables similar to the variables in the original reanalysis, is applied by including an additional nudging term in the tendency equation. The Newtonian nudging can be mathematically expressed as

$$\dot{X} = F(X) + \alpha(X - X_a) \quad (1)$$

In this expression F is the nonlinear model equation, α is the nudging coefficient, X is the model state variable, and X_a is the variable from reanalysis. Since reanalysis is provided every 6 h, X_a during the 6-h interval is linearly interpolated.

The model is also nudged toward the observed rain rates by modifying a specific humidity column. The PI technique enables the assimilation of TRMM rain rate into the FSUGSM using a reverse cumulus algorithm. The reverse algorithm generates constraints to restructure the distribution of moisture fields produced by the FSUGSM. Through the rainfall nudging, the humidity vertical profile experiences modifications as a function of the observed and predicted rain rates. As a result, model precipitation is brought closer to the observed rain rate. A vertical structure function (Nunes and Cocke 2004) is used for the modified moisture.

$$q_m = \frac{R_o}{R_p} q + \frac{(1/g) \int_{\sigma_t}^{\sigma_b} q d\sigma}{(1/g) \int_{\sigma_t}^{\sigma_b} d\sigma} \left(1 - \frac{R_o}{R_p}\right). \quad (2)$$

Here, q_m is the modified specific humidity, q is the specific humidity before PI, R_o and R_p are the observed and predicted rainfall rates and σ_b and σ_t denote σ the levels at the base and top of the clouds, respectively. However, the Kuo scheme, which constrains the regions where model rain rates are modified, requires convective instability and moisture convergence for the initialization. The modification is applied at every time step, but it is limited to 10 % for any one time step to prevent abrupt drift of the model state

variables. The rain rate nudging is not conducted unless the model produced or observed rain rates exceed 10 mm/day. Details of this procedure are described by Nunes and Cocke (2004).

During the integration, the optimum interpolation sea surface temperature (OISST) is used as a lower SST boundary condition and is updated weekly. Land surface conditions such as vegetation and snow depth are prescribed by their monthly climatology.

To examine the impact of the diurnal cycle on the MJO, we design two simulations that are identical in all aspects except the following. One simulation includes nudging of rain rate that varies at 3-h intervals and Newtonian nudging of dynamic variables from NCEP R2 at 6-h intervals (hereafter CTRL). The other simulation incorporates nudging of daily averaged TRMM rain rate and daily averaged prognostic variables from NCEP R2, applying the same nudging coefficients used in CTRL (hereafter NO_DIURNAL). To diminish the variability of the diurnal cycle in the NO_DIURNAL experiment, the daily averaged values of rain rate and relevant model variables described above are nudged every 3 h and every 6 h, respectively, in a form of incremental analysis update to prevent assimilation hock (Bloom et al. 1996). The diurnal cycle is not completely removed from the NO_DIURNAL because there is still diurnally varying radiation in both simulations. However, the applied Newtonian relaxation toward incorporated analysis acts as a constraint to accommodate corresponding heating associated with the assimilated convection. The rain rate nudging is conducted in an area extending from 50°S to 50°N; the dynamic nudging is conducted over the whole globe. The outputs from CTRL and NO_DIURNAL are examined for four austral summers (DJF), when the MJO is at maximum amplitude, from 2000/2001 to 2003/2004. In addition, the NO_NUDGING experiment, in which the rain rate nudging and Newtonian nudging are turned off, is also performed to evaluate the performance of the assimilation technique in FSUGSM.

2.3 Cyclostationary empirical orthogonal function (CSEOF) technique

A statistical analysis known as the CSEOF technique is used to verify whether the diurnally varying signal is discarded properly in the NO_DIURNAL experiment. First, empirical orthogonal function (EOF) analysis is performed on rainfall data from each experiment described above. Then, CSEOF analysis is conducted in the EOF space with a nested period of 1 day (equal to eight 3-h intervals). The first 100 EOFs are used as basis functions; together, the 100 EOFs explain above 80 % of the total variability.

In CSEOF analysis (Kim et al. 1996; Kim and North 1997), space–time data $T(r, t)$ are decomposed into

$$T(r, t) = \sum_n LV_n(r, t) PC_n(t) \quad (3)$$

where $LV_n(r, t)$ are cyclostationary loading vectors and $PC_n(t)$ are corresponding principal component time series. The cyclostationary vectors are periodic in time

$$LV_n(r, t) = LV_n(r, t + d) \quad (4)$$

where d is the nested period. Each $LV_n(r, t)$ in this study represents daily and subdaily physical evolution of the rain rate, and the corresponding PC time series describes the variation of the amplitude on time scales longer than a day.

2.4 Composite method

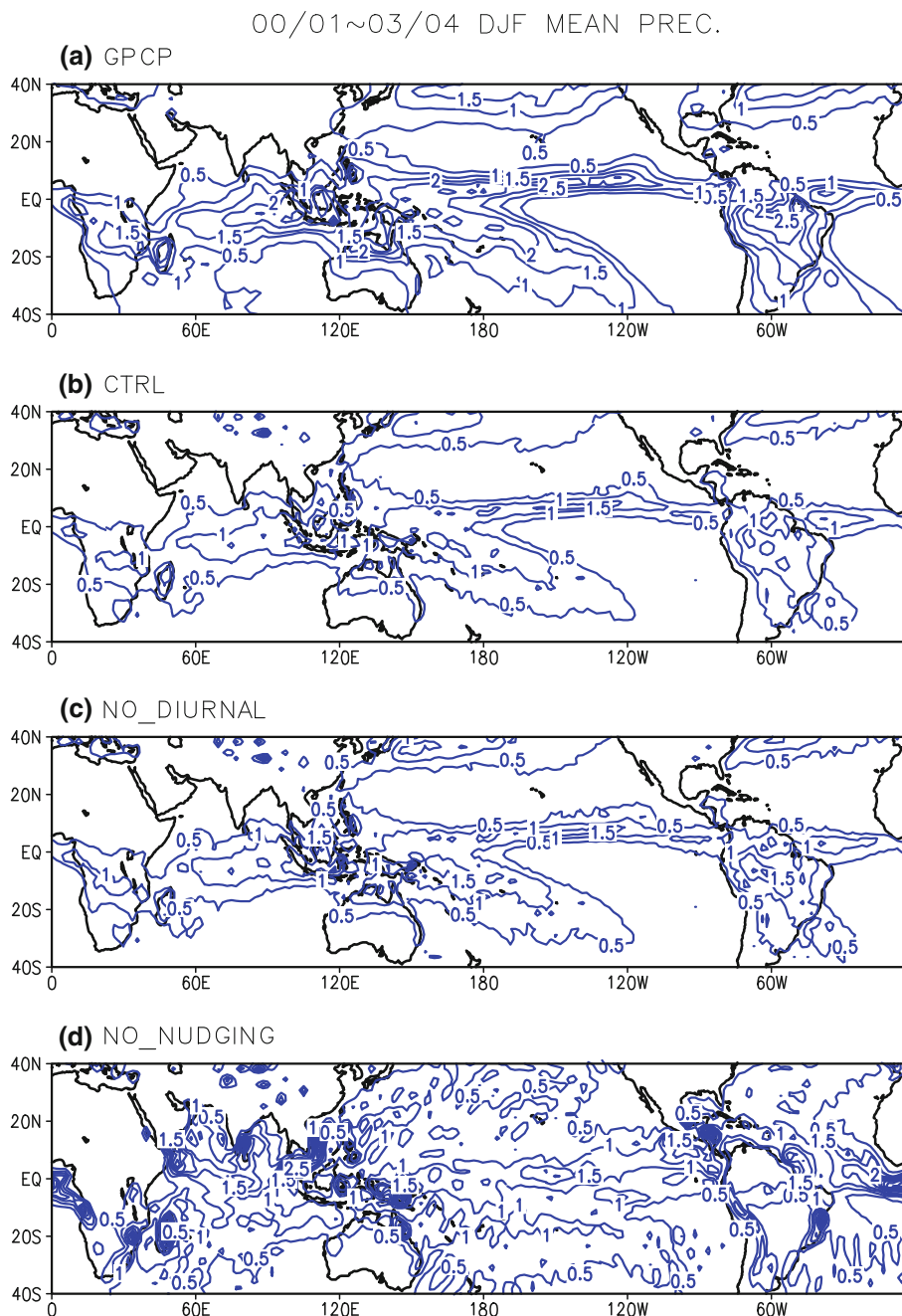
We adopt the Real-Time Multivariate MJO (RMM) index derived by Wheeler and Hendon (2004) for the composite analysis to analyze the MJO by comparing results from CTRL to those from NO_DIURNAL. The RMM index is based on a pair of EOFs of the combined fields of 850 hPa zonal wind, 200 hPa zonal wind, and satellite-observed outgoing longwave radiation (OLR) data averaged near the equator. Projection of the daily observed data onto the multi-variate EOFs, with the annual cycle and components of interannual variability removed, yields PC time series that vary mostly on the intraseasonal time scale of the MJO only. The pair of PC time series are called as RMM1 and RMM2, respectively. The RMM1 and RMM2 construct the two-dimensional phase space of MJO and represent the location of MJO in the phase space as a point (RMM1, RMM2). Distance of a point from the origin determines the amplitude of the MJO. The phase space is divided into eight sectors, from which the location of the MJO convective center between Africa and the eastern Pacific can be inferred. For composite analysis, only cases in which the amplitude of the MJO is greater than unity are chosen for four austral summer years (2000/2001–2003/2004).

3 Results

3.1 Climatological simulation

First, we investigate the mean state of precipitation as an essential starting point for evaluating model simulations; if the model simulation lacks the correct basic state, then we cannot necessarily guarantee a better simulation of the MJO (Slingo et al. 1996; Kemball-Cook et al. 2002). We validate the model simulations against the GPCP observed precipitation during the austral summer (DJF). Without physical initialization and dynamical nudging, the FSUGSM is rarely able to represent the realistic mean state (Fig. 1d). The rainfall distribution is noisy and the South Pacific

Fig. 1 Horizontal distributions of austral summer mean (December–February) precipitation (mm day^{-1}) from **a** GPCP, **b** CTRL, **c** NO_DIURNAL, and **d** NO_NUDGING. Contours are at every 0.5 mm day^{-1}

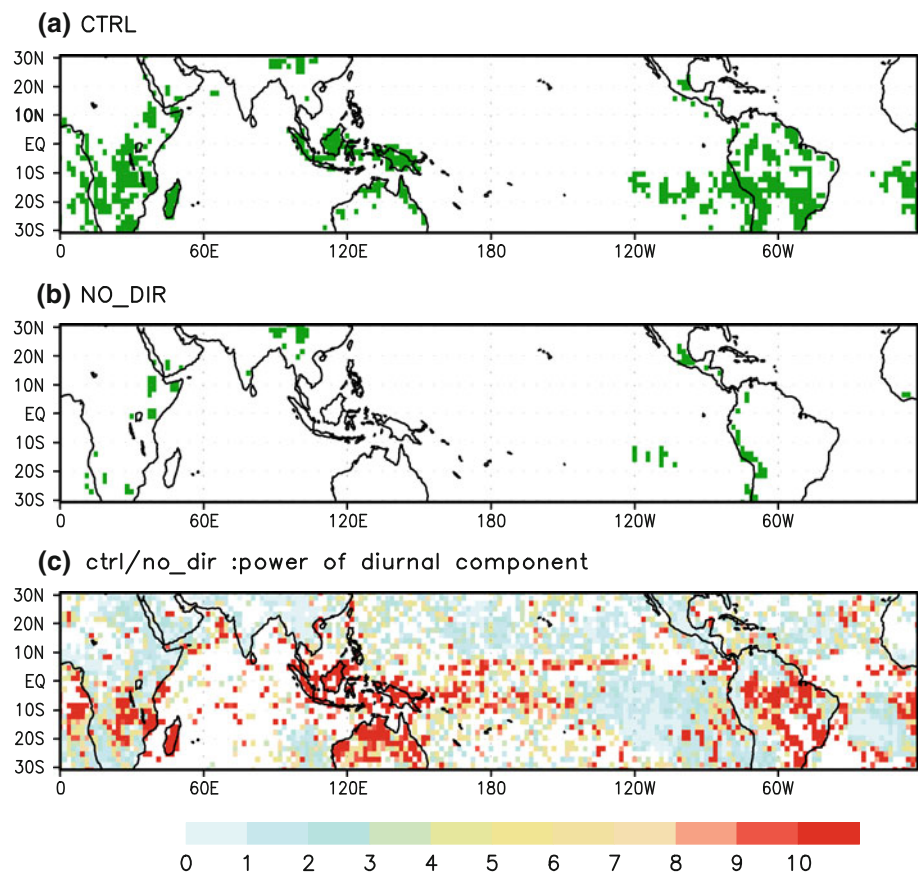


convergence zone (SPCZ) that extends southeastward is not shown clearly. Unlike the NO_NUDGING simulation, both the CTRL and NO_DIURNAL simulations show good agreement with the observed precipitation, although the simulations tend to underestimate the rainfall amounts.

Power spectra analysis is conducted on the time series of rainfall at each grid point (extending from 30°S to 30°N , globally) derived from the CTRL and NO_DIURNAL simulations. Figure 2a, b depict grid points where the diurnal cycle of rainfall has the largest significant power against the red noise background in the CTRL and NO_DIURNAL experiments, respectively. In CTRL, the

diurnal component is most dominant over the Maritime Continent, the northern edge of Australia, the middle of South America, and Southern Africa (Fig. 2a). In contrast, the diurnal cycle, which is prominent in CTRL, almost fades out in the NO_DIURNAL experiment (Fig. 2b). This implies that because of the assimilation of the daily averaged precipitation and other atmospheric variables into the FSUGSM, the diurnal signal is weakened enough to examine the intraseasonal variability without the diurnal cycle in the NO_DIURNAL simulation. Figure 2c displays the CTRL-to-NO_DIURNAL ratio of power in the diurnal band. The power of the diurnal component at greater than

Fig. 2 Spatial distribution where diurnal component of precipitation has maximum power during boreal winter (DJF) 2000/2001–2003/2004 in **a** CTRL and **b** NO_DIURNAL experiment. The ratio of power at diurnal band of CTRL to that of NO_DIURNAL is shown in **(c)**. The power of diurnal component greater than 95 % confidence level against red noise null hypothesis of each grid point from CTRL and NO_DIURNAL experiment is considered for the ratio



the 95 % confidence level against the red noise null hypothesis of each grid point from the CTRL and NO_DIURNAL experiments is considered for the ratio. Over 80 % of the domain shows the ratio greater than unity. This also supports the suppression of the diurnal cycle in the NO_DIURNAL simulation, especially over the Maritime Continent, which is the main region of interest.

In addition, we summarize the percentage of the region in the analysis domain (40°E–180°E, 15°S–15°N) where the CTRL-to-NO_DIURNAL ratio of not only precipitation but also of relevant variables such as humidity, zonal wind, and temperature exceeds unity in Table 1. It turns out diurnal components are suppressed over most of the analysis region.

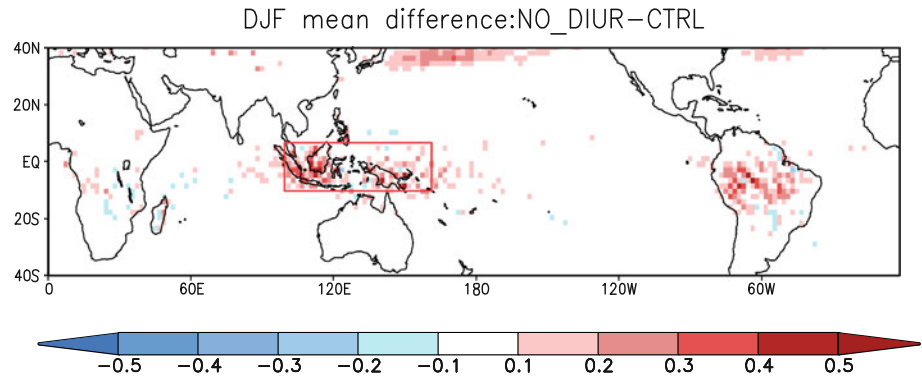
Figure 3 shows the differences in the DJF mean precipitation between the NO_DIURNAL and CTRL simulations. NO_DIURNAL produces more rainfall than CTRL, especially over the Maritime Continent (marked by the rectangular box in Fig. 3) and the middle of South America. Deliberately eliminating the diurnal component in the NO_DIURNAL simulation could closely relate to the increase in the seasonal mean rainfall amount over the Maritime Continent. We deduce that the difference originates from the strong diurnal signal over the Maritime Continent.

Table 1 Percentage of grid where the CTRL-to-NO_DIURNAL ratio of power in diurnal band greater than unity (40°E–180°E, 15°S–15°N)

Variables	Percentage (%)
Lower levels integrated MSE	87.4
Vertically iterated MSE	82.4
Precipitation	84.6
Pressure velocity (500 hPa)	92.8
Zonal wind (850 hPa)	97.2
MSE (850 hPa)	78.4
Specific humidity (1,000 hPa)	80.7
Temperature (1,000 hPa)	98.6
MSE (1,000 hPa)	88.2
Evaporation	86.5

We analyze three-hourly precipitation from each experiment, applying CSEOF analysis to ensure that the diurnal signal is suppressed sufficiently in the NO_DIURNAL simulation, and examine how diurnal variations of rainfall over the Maritime Continent are represented in CTRL and NO_DIURNAL, respectively. Figures 4 and 5 display the first CSEOFs, which represent the diurnal cycle of rainfall in the austral summer (DJF) over the Maritime Continent in CTRL and NO_DIURNAL, respectively.

Fig. 3 Difference in the DJF mean precipitation between CTRL and NO_DIURNAL experiments (mm day^{-1})



The diurnal rainfall evolution shows a substantial difference between the land and the sea in CTRL (Fig. 4). Whereas precipitation over the islands (e.g., Borneo, Sumatra, Sulawesi, and New Guinea) reaches a maximum in the evening (2000–0200 LST (Local Standard Time); Fig. 4e–g) and a minimum in the morning and early afternoon (0800–1400 LST; Fig. 4a–c), precipitation over the seas (e.g., the South China Sea and the Java Sea) reaches its peak in the early morning (0500–1100 LST; Fig. 4a, b, h). The rainfall migrations offshore at dawn and inland in the early afternoon are also revealed. These

results are consistent with the results of previous studies that were based on different datasets (Kikuchi and Wang 2008; Mori et al. 2004; Ichikawa and Yasunari 2006, 2008; Rauniyar and Walsh 2011). Since the land surface has a lower heat capacity, temperature variation caused by solar heating is more significant over the land than over the ocean. However, since we use weekly updated SST as a lower SST boundary condition, this physical process will not be represented completely in model simulations. When the sun rises, the temperature over the land increases rapidly until the sun reaches its maximum altitude. This causes

Fig. 4 Temporal evolution of the 1st CSEOF mode (the seasonal cycle) of rainfall (mm per 3 h) over the Maritime Continent from CTRL

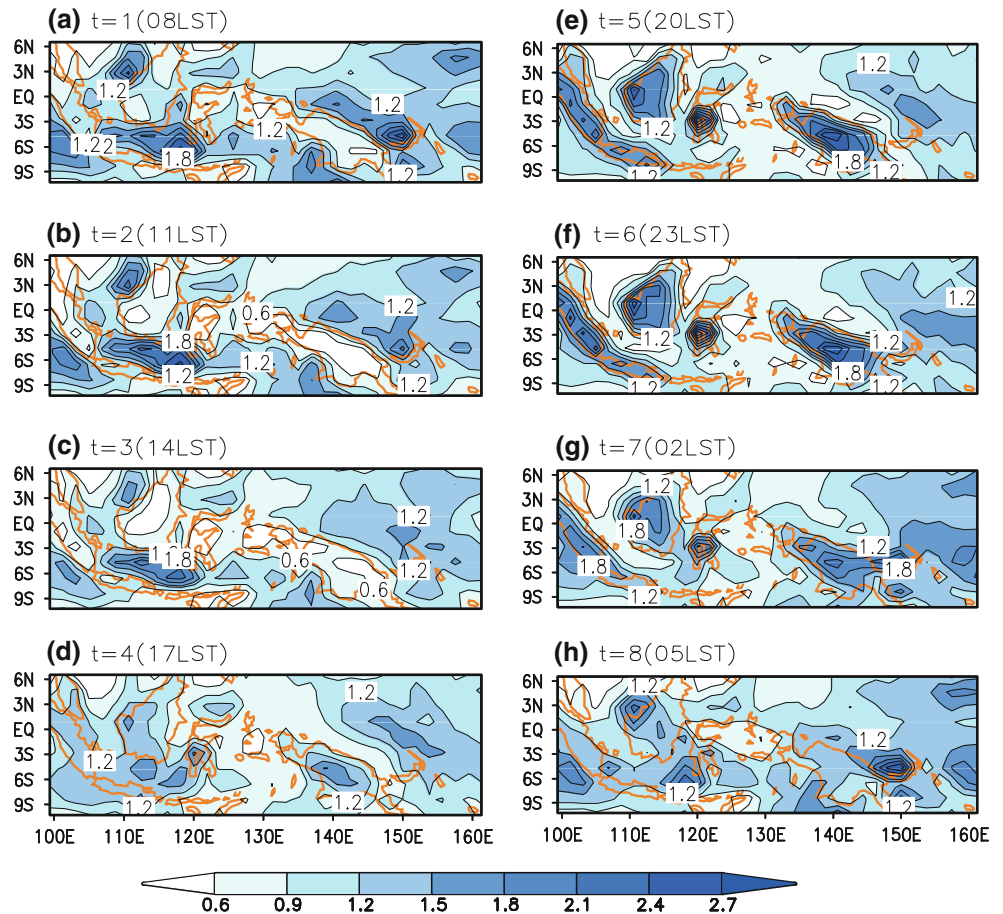
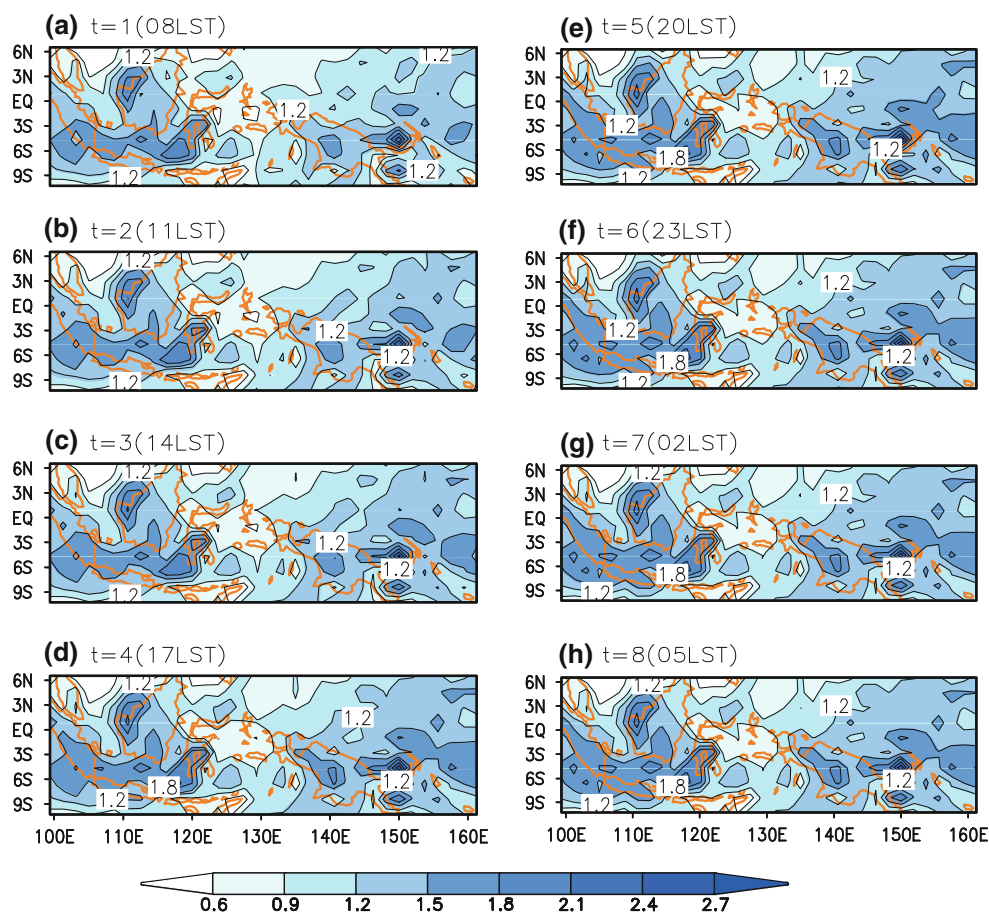


Fig. 5 Same as Fig. 4, but for NO_DIURNAL



pressure gradients between the land and the ocean and the static destabilization of the atmosphere (Bowman et al. 2005; Yang and Smith 2006). The situation reverses after sunset. The pressure gradient induces daytime sea breezes, resulting in a moisture supply and a forced ascent of air. The land–sea breeze often plays an important role in the rainfall differences between the land and the ocean in fine temporal and spatial scales (Qian 2008). Remarkably, both the distinct land–sea contrast in the diurnal cycle of rainfall and the propagation of rainfall bands clearly depicted in CTRL disappear in the NO_DIURNAL simulation (Fig. 5). Figure 6 displays one-day averaged precipitation from CTRL. The overall spatial pattern of rainfall in each panel of Fig. 5 is consistent with the rainfall pattern in Fig. 6 although the rainfall amounts differ. Therefore, discrepancies between CTRL and NO_DIURNAL are caused by nudging the daily averaged fields in the NO_DIURNAL simulation in an attempt to suppress the diurnal variability.

3.2 Influence of the diurnal cycle on the MJO

Before focusing on the impact of the diurnal cycle on the MJO, it is necessary to assess the skill of the FSUGSM with the assimilation technique in simulating the intraseasonal

oscillation. Figure 7 shows the composite spatial patterns of precipitation variability captured by the RMM index. The results from the CTRL experiment (left) are compared to those from the GPCP observation (right). The CTRL composite shows the robust eastward-propagating MJO as being comparable to the MJO in the GPCP data. The salient features of the MJO are also shown in the CTRL composite (Hendon and Salby 1994; Seo and Kim 2003; Wheeler and Hendon 2004). The MJO convection initiated over the western Indian Ocean in phase 1 propagates eastward and approaches the western part of the Maritime Continent near Sumatra, Borneo, and the Java Sea in phase 3. During phases 3–5, the convectively enhanced phase of the MJO approaches and then resides over the Maritime Continent. In phases 6–8, suppressed convection passes over the Maritime Continent. These DJF composite patterns based on the RMM index show evolutionary features of the MJO similar to features in previous studies (e.g., Wheeler and Hendon 2004). Therefore, we conclude that the FSUGSM used in this study adequately represents the MJO, allowing us to concentrate solely on the influence of the diurnal cycle regarding the simulation of the MJO.

Figure 8 shows phase–longitude diagrams of composite precipitation anomalies of the CTRL (upper) and

Fig. 6 The daily averaged 1st CSEOF mode of precipitation (mm per 3 h) from CTRL

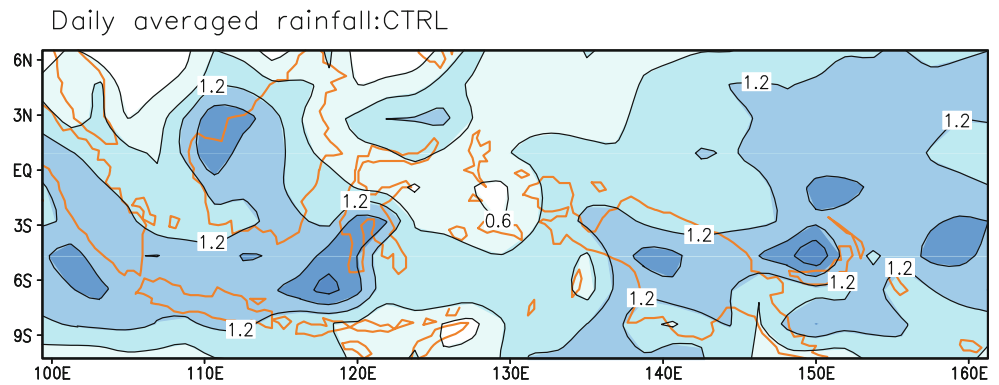
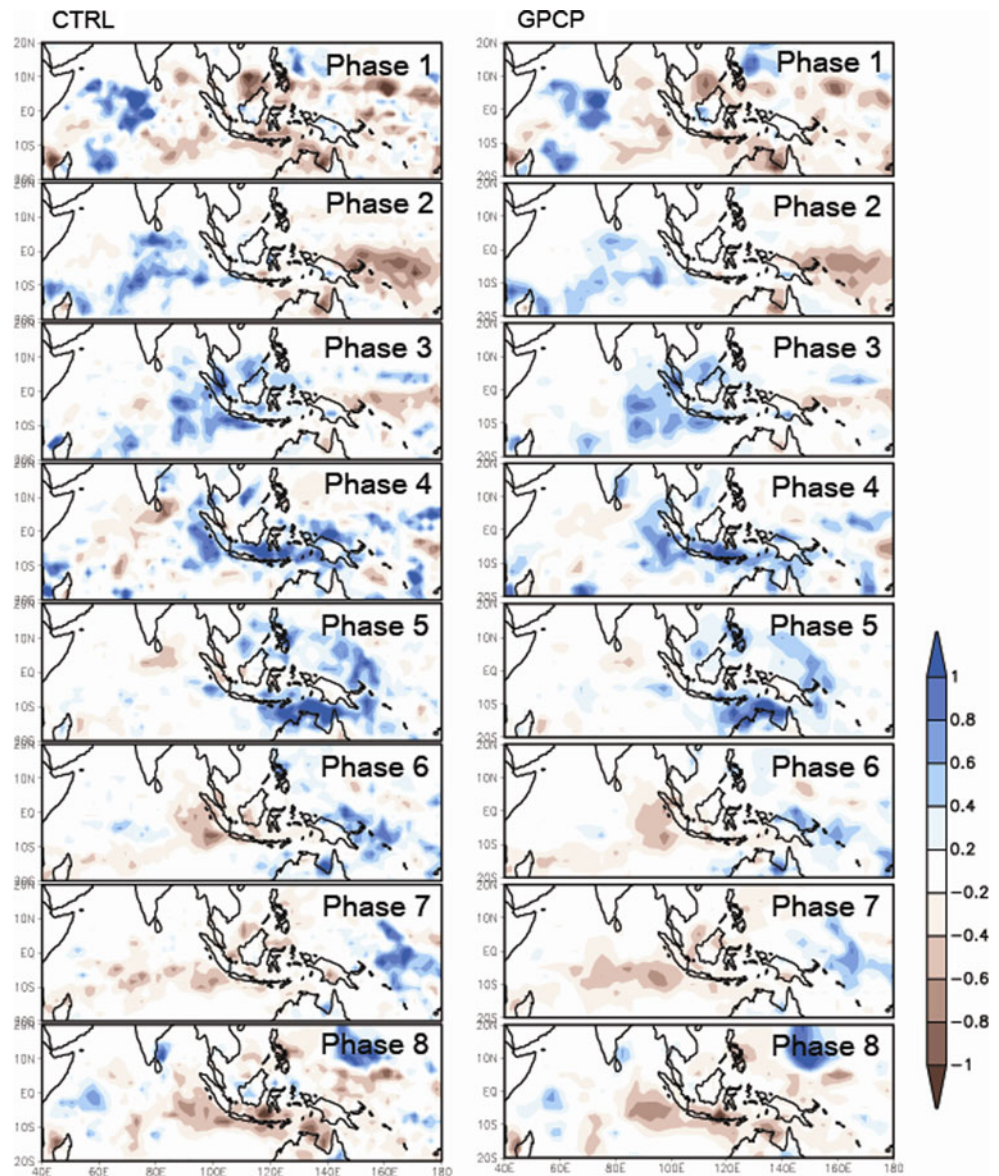


Fig. 7 DJF composite precipitation anomalies (mm day^{-1}) of CTRL experiment (left) and GPCP observation (right)



NO_DIURNAL (lower) experiments. The diagram clearly depicts the origination of the convection anomalies over the western Indian Ocean and their eastward propagation.

Positive precipitation anomalies (red) are followed by negative rainfall anomalies (blue). In CTRL, the convective anomaly becomes considerably weaker while passing over

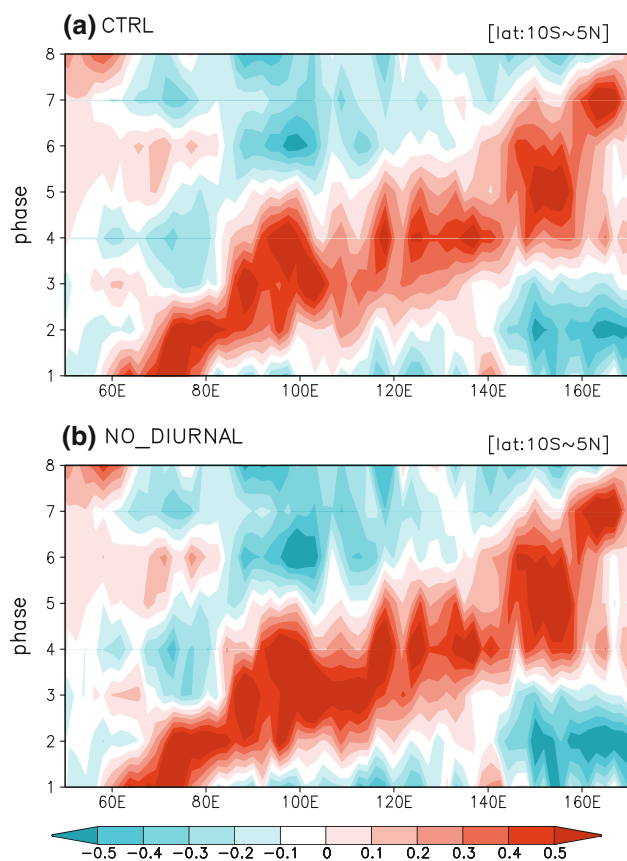


Fig. 8 Phase-longitude diagrams of composite precipitation anomalies (mm day^{-1}) for **a** CTRL and **b** NO_DIURNAL experiments. Phases are from the MJO life-cycle composite and values are averaged between 10°S and 5°N

the Maritime Continent (100°E – 120°E) during phase 3, as a number of previous studies have pointed out (Seo and Kim 2003; Inness and Slingo 2006; Kim et al. 2009), and it redevelops over the west Pacific. In contrast, the weakening of the convective precipitation is absent over the Maritime Continent region in the NO_DIURNAL simulation.

Figure 9 shows the difference in composites of precipitation anomalies between CTRL and NO_DIURNAL with respect to the MJO phase. Of interest are the negative values over the Maritime Continent in phase 3, during which the active MJO convection impinges on the western Maritime Continent (Sumatra, Borneo, and Sulawesi). This implies that compared to the CTRL experiment, more precipitation falls when the convectively enhanced phase of the MJO is located over the Maritime Continent in NO_DIURNAL. On the other hand, during the suppressed phases of the MJO (phases 5–1), when negative rainfall anomalies reside mainly over the Maritime Continent, the amplitude of these negative anomalies is larger in NO_DIURNAL than in CTRL.

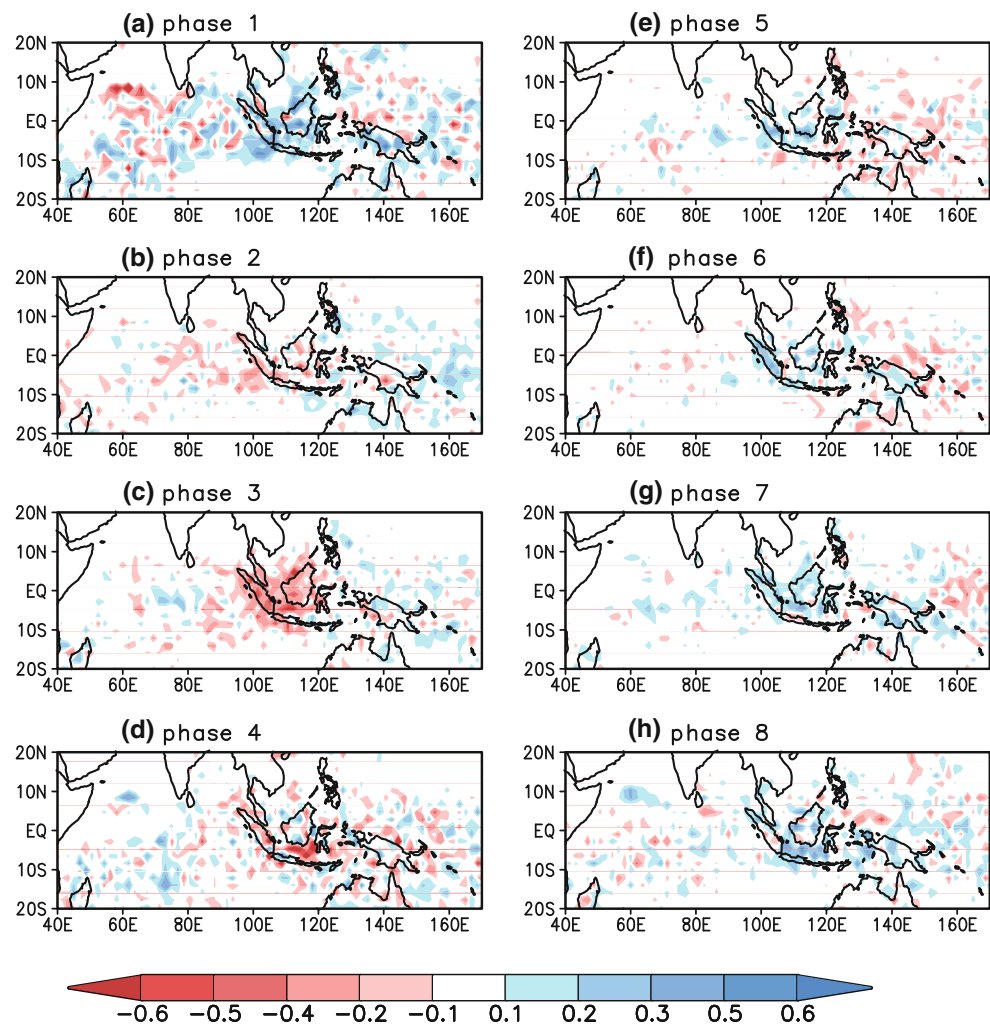
To further examine influences that removing the diurnal cycle has on the simulation of the intraseasonal variability

in terms of the magnitude and geographical distribution, plots of the variance of 40–80-day filtered precipitation in CTRL and NO_DIURNAL are given in Fig. 10. This figure can be compared to Fig. 3 of Kim et al. (2009). Their figure is derived for November through April, and they used a 20–100-day bandpass filter to assess the performances of various models in simulating the MJO. CTRL shows a pattern similar to the CMAP observation in their Fig. 3, resulting in reduced intraseasonal variability over the Maritime Continent (Fig. 10a). In contrast, large intraseasonal variance extends over the Maritime Continent in the NO_DIURNAL simulation (Fig. 10b).

Figure 11 shows wave number–frequency plots (Hayashi 1979) of precipitation and 850-hPa zonal wind in CTRL (Fig. 11a) and NO_DIURNAL (Fig. 11b), respectively. The wave number–frequency analysis is useful for separating phenomena in the time–longitude domain into westward- and eastward-moving components (Wheeler and Kiladis 1999). Using this method, we interpret dynamical attributes of deep tropical convection regarding the dispersion relations of particular wave modes. Zonal wave numbers 1–3 are evident in precipitation and zonal wave number 1 is dominant in zonal wind at 850 hPa for periods of 45–50 days in CTRL and NO_DIURNAL. This result is quite similar to the observational result of Kim et al. (2009). Waves within these scales can be considered the MJO (Wheeler and Kiladis 1999). Worth noting is that the assimilation of the daily averaged fields has no impact on periods of dominant waves; however, it does affect the power of rainfall. Comparing the power of rainfall and the zonal wind at 850 hPa for periods of 45–50 days between CTRL and NO_DIURNAL, we find an increase in the power of rainfall in NO_DIURNAL compared with CTRL. We find no significant change in the power of zonal wind at 850 hPa in either experiment. From these results, we deduce the removal of the diurnal component exerts more direct influence on the thermodynamic process rather than on the dynamic process related to the evolution of the MJO.

We analyze divergence, specific humidity, zonal wind, and pressure velocity anomalies relevant to the MJO. Composite variables averaged over the Maritime Continent with respect to phase are shown in Fig. 12. Time series exhibit general aspects of dependency on the evolution of the MJO convection. For example, when convection starts to develop in phase 3 over the Maritime Continent, the wind begins to change from easterly to westerly, as observed in previous studies (e.g., Seo and Kim 2003), and lower level convergence and upward motion at 500 hPa intensify, accompanied by an increase in the humidity. In comparison with CTRL, as pointed out above, area-averaged precipitation from the NO_DIURNAL experiment increases during the active phases (3–4) of the MJO.

Fig. 9 Spatial distribution of the difference in composite precipitation anomalies (mm day^{-1}) between CTRL and NO_DIURNAL with respect to the MJO phase



Analogously, vertical motion at 500 hPa, convergence at 1000 hPa, and specific humidity at 700 hPa in the NO_DIURNAL experiment have larger values than those same variables from CTRL during convectively active phases (Fig. 12c–e). In contrast, zonal wind at 850 hPa shows little difference between the NO_DIURNAL and the CTRL experiments regardless of phase.

These results suggest that the deliberate suppression of the diurnal signal during the integration gives rise to an amplification of the MJO without changing propagating speed, especially over the Maritime Continent where the prominent diurnal cycle exists. Because the same wind and convection are nudged toward observation and reanalysis in the daily time scale, the propagation speed cannot be changed by the experimental design.

3.3 How does the suppressed diurnal cycle affect the mean state of rainfall?

Since it is well known that simulation of the MJO is linked with that of the background mean state (Slingo et al. 1996),

we started our research by comparing the simulations of mean state by CTRL and NO_DIURNAL, shown in Figs. 1 and 3. As a result, we find that the simulation with a suppressed diurnal cycle reproduces a larger amount of the mean precipitation over the Maritime Continent than does the simulation with the general diurnal cycle. Prior to performing the detailed analysis on the impact of the modulation of the diurnal cycle on the MJO simulation, it is essential to investigate the physical mechanism behind the increase of seasonal mean precipitation in the NO_DIURNAL experiment. Since cumulus parameterization in the model plays the most important role in the precipitation process, it is helpful to examine the convective instability and moisture convergence, which are key components of the modified Kuo scheme used in this study (Sect. 2.2).

First, we compare convective instability, defined as the difference between equivalent potential temperature at 500 and 850 hPa (Sato and Kimura 2005), as shown in Fig. 13. Larger vertical differences of equivalent potential temperature over the Maritime Continent are more prevalent in NO_DIURNAL than in the CTRL simulation, which

Fig. 10 Variance of 40–80 day band-pass filtered precipitation ($\text{mm}^2 \text{day}^{-2}$) during austral summer (DJF) 2000/2001–2003/2004

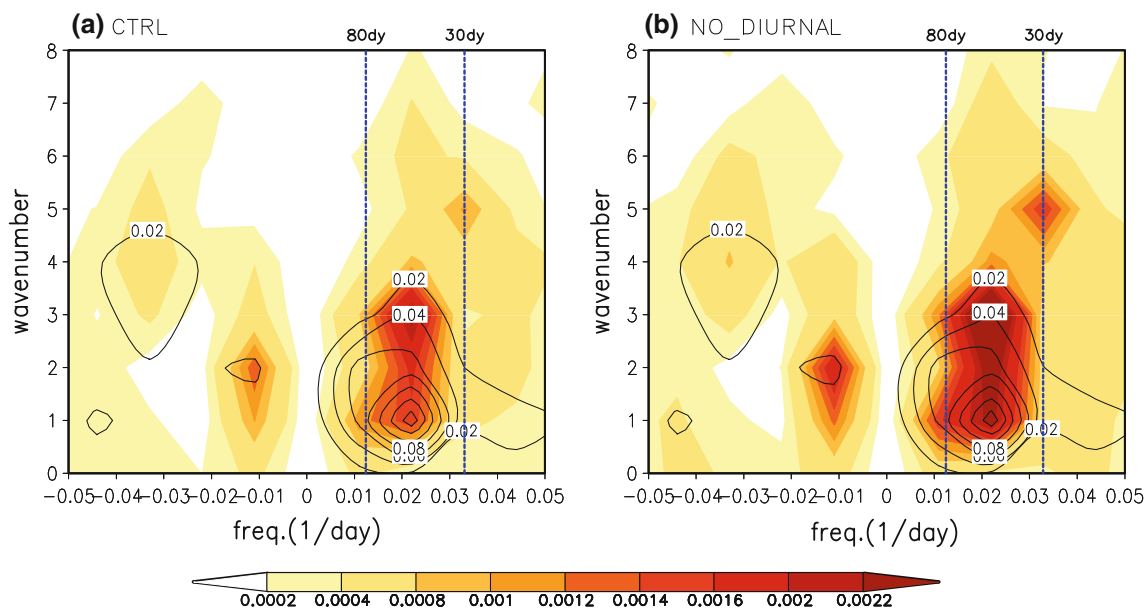
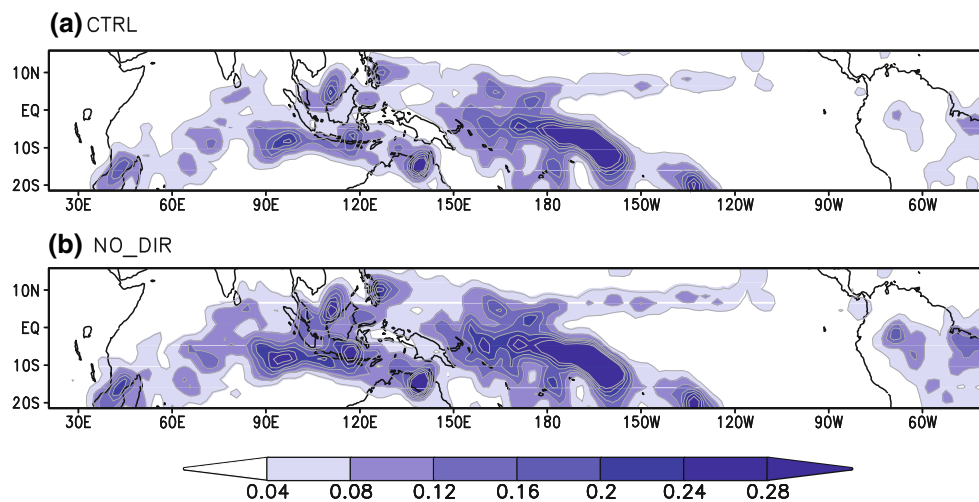


Fig. 11 DJF wavenumber–frequency spectra of 10°S – 10°N averaged precipitation ($\text{mm}^2 \text{day}^{-2}$) (shaded) and 850-hPa zonal wind ($\text{m}^2 \text{s}^{-2}$) (contour) for **a** CTRL and **b** NO_DIURNAL simulations

indicates more conditional instability exists in the NO_DIURNAL simulation. Figure 14 shows diurnal variation of the convective instability in the CTRL experiment (left column: a, b, c, d) and in the NO_DIURNAL experiment (right column: e, f, g, h). In the CTRL experiment, the air above the land areas of the Maritime Continent becomes unstable at 06 UTC, which corresponds to approximately 14 LST. The convective instability provides favorable conditions for late afternoon precipitation over land areas as shown in Fig. 4d–g. On the other hand, the assimilation of the daily averaged variables from reanalysis and rain rates results in persistence of convective instability all day long, even though instability increases at 06 UTC over the land areas of the Maritime Continent.

Second, Fig. 15 shows the diurnally varying moisture convergence along with the differences of the magnitude between the CTRL and the NO_DIURNAL experiments. From 00 UTC to 06 UTC, NO_DIURNAL simulates stronger moisture convergence over the Maritime Continent than the CTRL run does. However, from 12 UTC, which is when late afternoon and evening rainfall occurs over the land, the moisture convergence over Sumatra, Java, and New Guinea in CTRL becomes stronger than the convergence in the NO_DIURNAL simulation. Figure 16 presents the overall increase of moisture convergence in NO_DIURNAL compared to the CTRL run during the analysis period. On the basis of these results, we speculate that convective instability and moisture convergence are

Fig. 12 Composites averaged over the Maritime Continent (10°S–5°N, 100°E–160°E) for CTRL (black solid line) and NO_DIURNAL (grey dotted line) with respect to the MJO phase: **a** precipitation (mm per 3 h), **b** zonal wind (m s⁻¹) at 850 hPa, **c** pressure velocity (Pa s⁻¹) at 500 hPa, **d** divergence at 1000 hPa (s⁻¹), and **e** specific humidity (g kg⁻¹) at 700 hPa. Seasonal cycles are all removed before composites

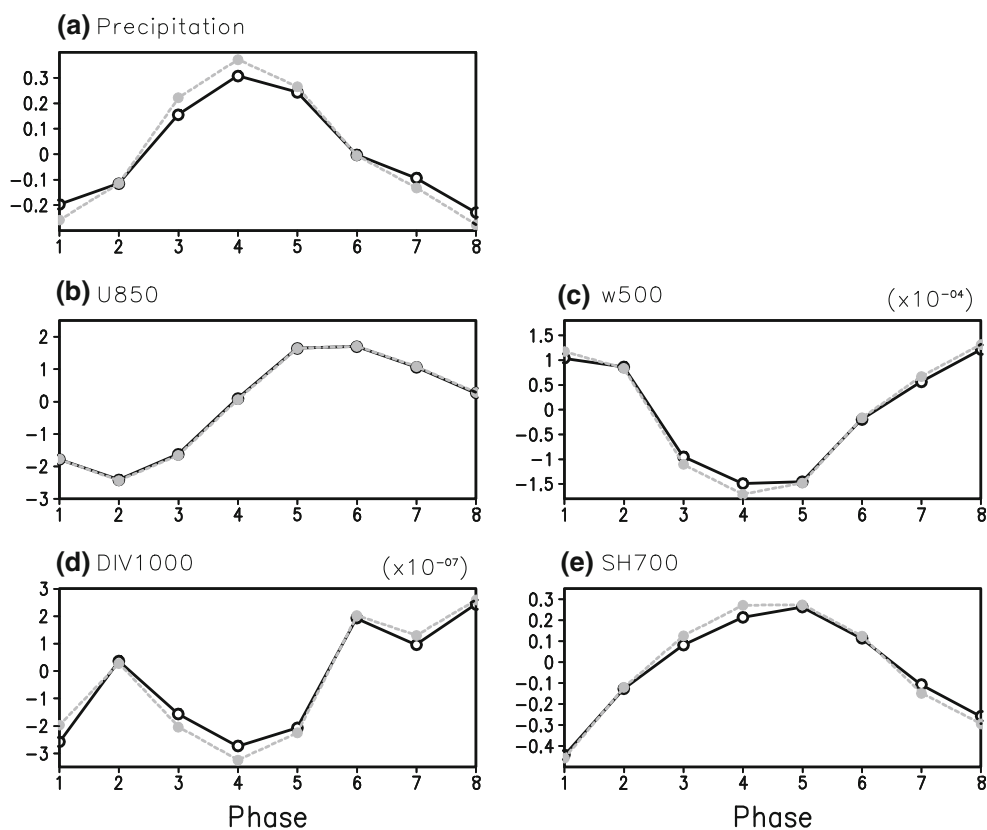
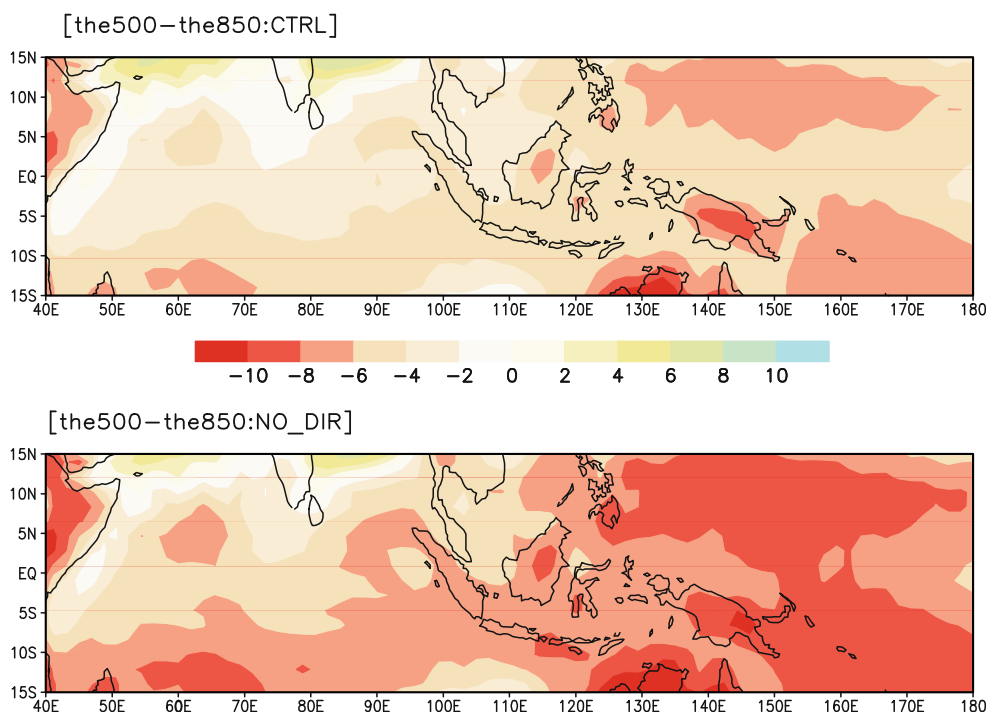


Fig. 13 Convective instability, defined as the difference of the equivalent potential temperature at 500 and 850 hPa, in CTRL (top) and NO_DIURNAL (bottom) averaged during boreal winter (DJF) 2000/2001–2003/2004



quite evenly distributed in time because the assimilation of daily averaged values during model integration of NO_DIURNAL differs from the CTRL simulation, which resolves distinct diurnal change of convective instability

and moisture convergence. As a result, the assimilation of the daily averaged variables seems to satisfy the requirements, e.g., convective instability and moisture convergence (Nunes and Cocke 2004) for physical initialization,

Fig. 14 Diurnal variation of convective instability (K) in CTRL (a–d) and NO_DIURNAL (e)–(h) during boreal winter (DJF) 2000/2001–2003/2004. The time in parenthesis denotes the corresponding local time of Maritime Continent

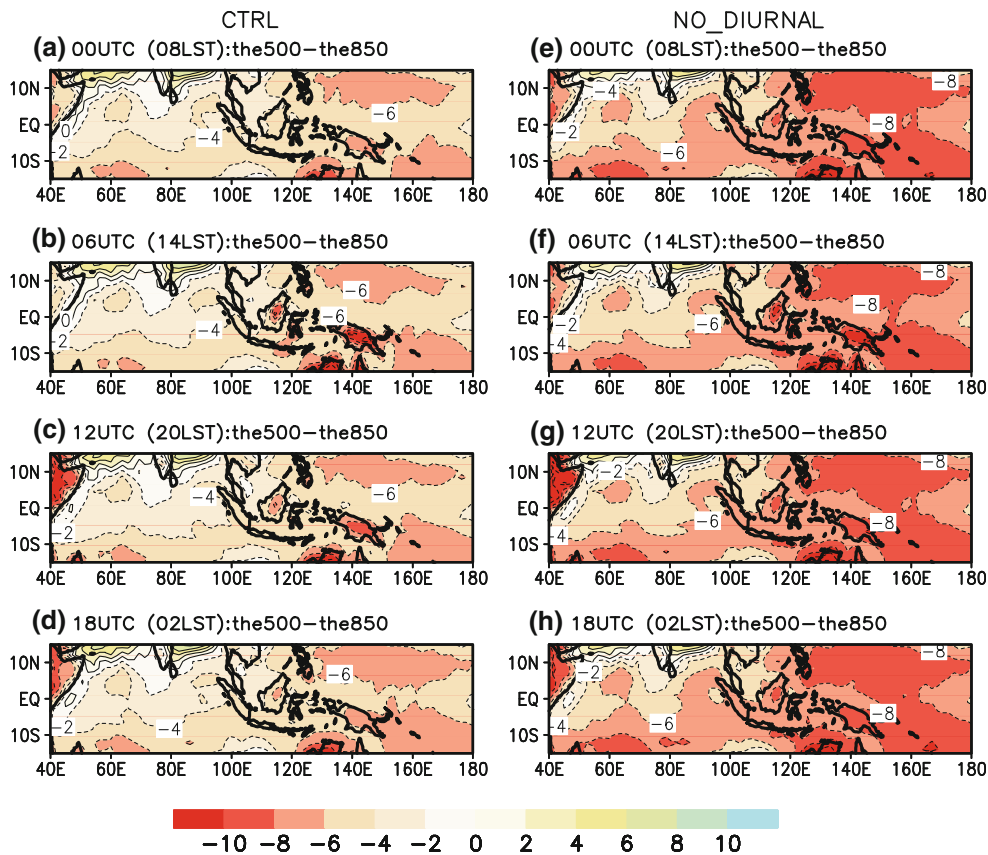
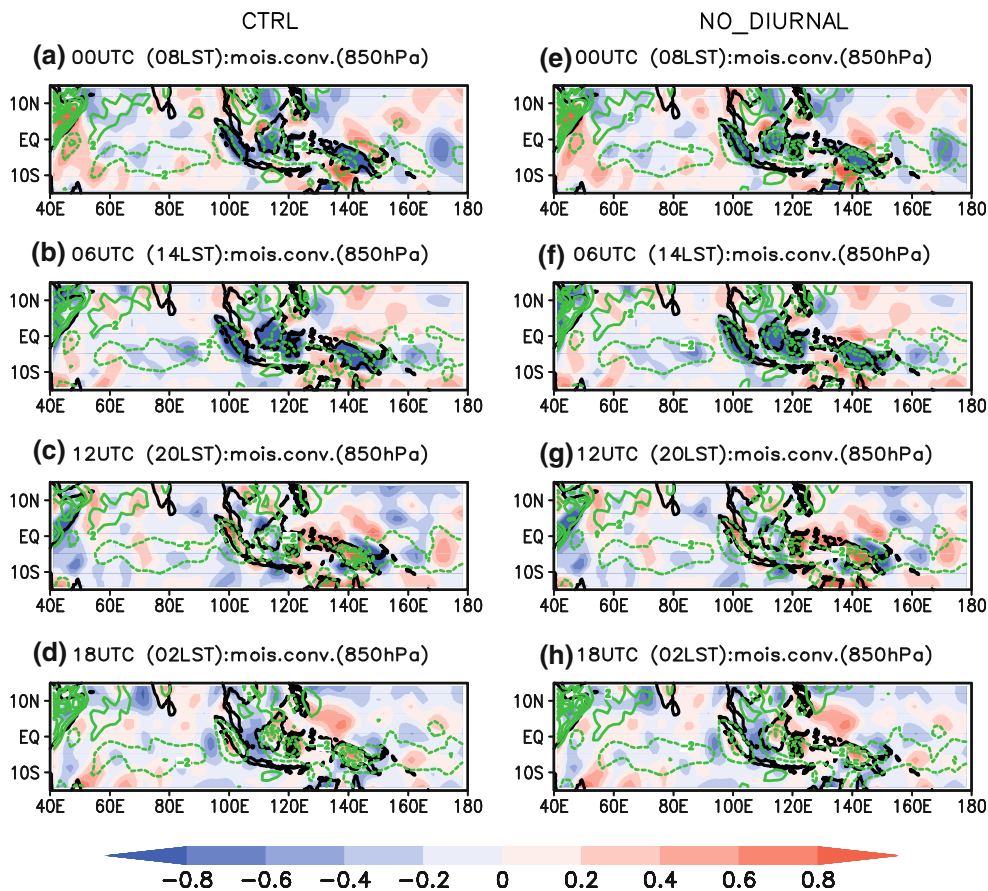


Fig. 15 Diurnal variation of moisture convergence at 850 hPa (contour: 10^{-5} g/kg/s) in CTRL (a)–(d) and NO_DIURNAL (e)–(h) during boreal winter (DJF) 2000/2001–2003/2004. The time in parenthesis denotes the corresponding local time of Maritime Continent. Zero line is omitted. The shaded areas denote corresponding difference of magnitude of moisture convergence between CTRL and NO_DIURNAL experiment at each time



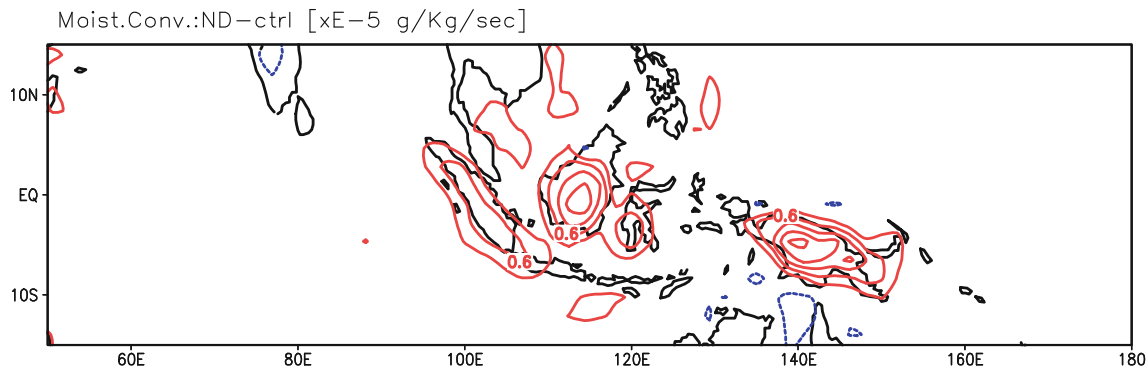


Fig. 16 Difference of magnitude of moisture convergence between NO_DIURNAL and CTRL experiment averaged during boreal winter (DJF) 2000/2001–2003/2004

which enables more frequent assimilation of moisture. Accordingly, this more frequent assimilation of moisture may contribute to the increase of mean precipitation over the Maritime Continent in the NO_DIURNAL simulation.

3.4 How does the suppressed diurnal cycle maintain the amplitude of the MJO over the Maritime Continent?

Using the detailed comparison of the MJO produced by the CTRL and NO_DIURNAL model simulations, we have demonstrated that diminishing the diurnal cycle during the model integration does produce an intensified MJO over the Maritime Continent. The question then becomes, which driving mechanism causes this difference? To answer the question, we must consider the theories regarding the development of MJO convection. Although theories based on observations and modeling studies have been suggested to explain the development of the MJO and its characteristics, fundamental understanding of the physical mechanism underlying the MJO remains elusive (Zhang 2005). A recharge-discharge theory (Bladé and Hartmann 1993) is one of the possible mechanisms that explains the evolution of the MJO. According to the paradigm, buildup of a column of moist static energy (MSE) occurs before MJO deep convection, and MSE is discharged during and after MJO convection (Bladé and Hartmann 1993; Kemball-Cook and Weare 2001; Maloney 2009). MSE is defined as $h = C_p T + gz + Lq$ where C_p is the specific heat of air, T is air temperature, g is the gravitational constant, z is the geopotential height, L is the latent heat of condensation, and q is the specific humidity. The first term on the right side of MSE denotes the enthalpy per unit mass of air. The second term is the potential energy, and the third term is the latent heat content. The first two terms stand for the dry static energy. When air rises dry adiabatically, enthalpy is converted into potential energy and latent heat content remains constant. In saturated adiabatic ascent, energy is exchanged among all

three terms. While the enthalpy and latent heat decrease, potential energy increases. Therefore, MSE is a useful property for examining the energy available to a parcel in the convective area on the basis of moisture and temperature in terms of not only the MJO but also the diurnal cycle. MSE is approximately conserved in the air parcels, even as they undergo phase changes between vapor and liquid, including the precipitation process (Back and Bretherton 2006). Atmospheric convection vertically rearranges MSE, but does not affect the column-integrated MSE.

Figure 17 shows the composite vertical distribution of the intraseasonal MSE anomalies at 115°E as a function of the MJO phase. Recall the result presented in Fig. 8 showing an apparent discrepancy between CTRL and NO_DIURNAL in the amount of rainfall anomalies near 115°E at phase 3. The overall vertical distributions are quite similar to those explained by previous studies (e.g., Kemball-Cook and Weare 2001; Maloney 2009) and in agreement with the recharge-discharge theory of the MJO. Positive MSE anomalies appear at lower levels (1000 hPa–950 hPa) in advance of the rainfall peak (phases 1–2). At phase 3, these anomalies build upward to 850 hPa. Positive anomalies in MSE peak in the middle troposphere at phase 4 consistent with the phase of the maximum positive precipitation anomalies over the Maritime Continent. Negative MSE anomalies reach their maxima at phase 6, during which the peak in negative rainfall anomalies occurs over the Maritime Continent, as shown in Fig. 8. A noticeable difference of magnitude in positive MSE anomaly peaks exists between CTRL and NO_DIURNAL in the lower troposphere. The MSE anomaly peak in NO_DIURNAL is 450 J kg^{-1} at 850 hPa during phase 3, which is 100 J kg^{-1} larger than the anomaly peak in CTRL. According to Kemball-Cook and Weare (2001), the MJO is partially controlled by the buildup and discharge of the low-level MSE. Therefore, Fig. 14 suggests that the larger positive MSE anomalies in NO_DIURNAL contribute to the intensification of the MJO over the Maritime Continent.

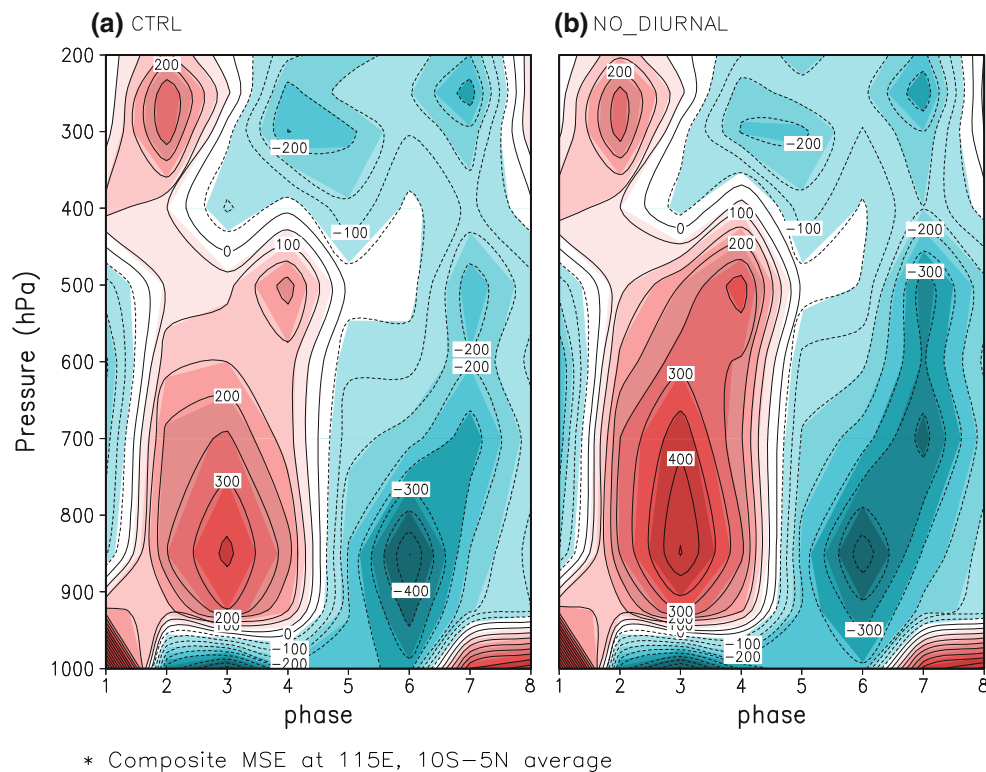


Fig. 17 Composite equatorial (10°S – 5°N averaged) intraseasonal moist static energy anomalies at 115°E from **a** CTRL and **b** NO_DIURNAL. The contour interval is 50 J/kg

We also investigate the convective instability over the Maritime Continent in terms of the evolution of the MJO in Fig. 18. The upper panel in Fig. 18 shows the composite of the absolute values after subtracting the convective instability of CTRL from that of NO_DIURNAL at MJO phase 3. A wider range of the larger conditional instability exists in NO_DIURNAL compared to the CTRL simulation. The lower panel in Fig. 18 shows the variation of the convective instability over the Maritime Continent in each simulation with respect to the MJO phase. The larger the absolute value exhibited by the time series, the more unstable the condition it indicates. Whereas stronger instability occurs during the developing and enhanced MJO phases (1–3), the instability decreases when suppressed MJO convection approaches the Maritime Continent at phase 6. The NO_DIURNAL maintains stronger convective instability than CTRL does throughout the MJO life cycle. The difference of the instability has maximum value during phase 3 consistent with the increase of the MSE difference shown in Fig. 8.

Moisture convergence in the boundary layer is one of the important factors that provides favorable conditions for the development of MJO convection (Maloney and Hartmann 1998; Zhang 2005). Low-level convergence provides an upward flux of moisture by increasing the low-level equivalent potential temperature through moistening. We

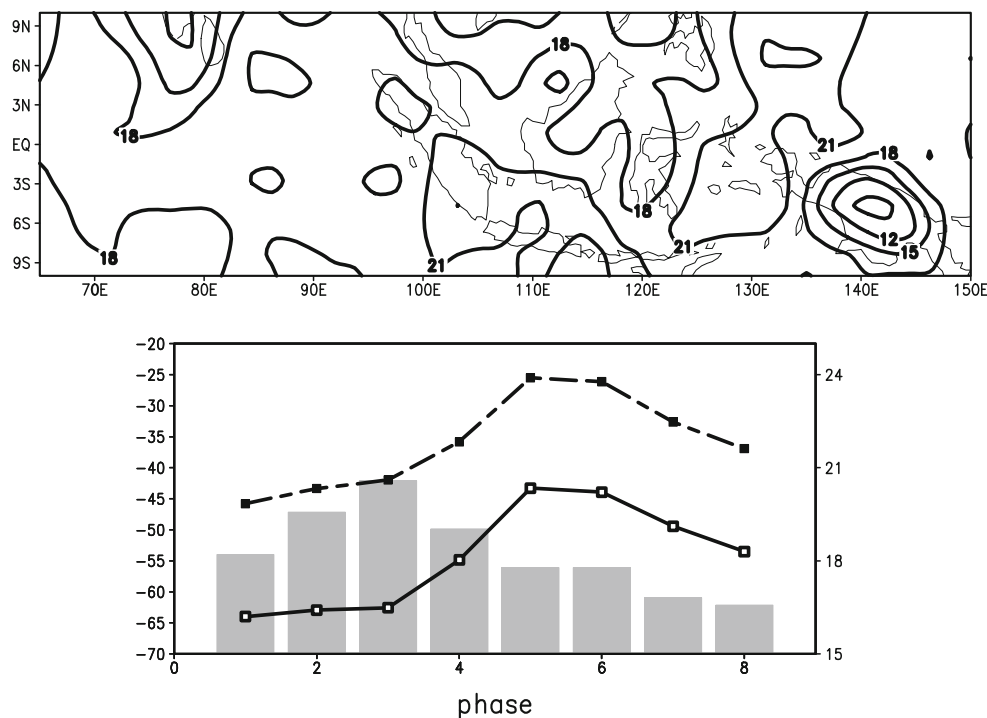
compute the difference of the moisture convergence at 850 hPa between the NO_DIURNAL and the CTRL experiments (Fig. 19). Moisture converges more strongly over the Maritime Continent in NO_DIURNAL than it does in the CTRL simulation. Larger instability and stronger moisture convergence provide a condition conducive for the development of convection.

Thus, the amplification of the MJO over the Maritime Continent in the NO_DIURNAL experiment may be inferred from the combined effect of the increased buildup of MSE, a more convectively unstable condition, and stronger moisture convergence revealed in the NO_DIURNAL simulation.

4 Summary and discussion

In the present study, we use modeling experiments to investigate the impact of the diurnal cycle on the MJO during the Australian summer. Physical initialization and a nudging technique enable us to assimilate observed TRMM rain rate and atmospheric variables from the NCEP R2 into the FSUGSM, resulting in a realistic simulation of the basic climatology of rainfall during austral summer (DJF) and the MJO. We modulate the diurnal cycle from the model integration by assimilating daily averaged fields of precipitation, surface pressure, temperature, vorticity, divergence,

Fig. 18 Composite of the daily mean convective instability difference between NO_DIURNAL and CTRL experiment at MJO phase 3 (top) and daily mean convective instability averaged over lat:10°S–5°N, lon:100°E–120°E (bottom) with respect to MJO phase. Dashed line represents CTRL and solid line represents NO_DIURNAL simulation. Y-axis on the left denotes the convective instability. Bar graph represents the difference of the convective instability between NO_DIURNAL and CTRL at each MJO phase



difference of mag. moist. conv: ND-CTRL (phase 3)

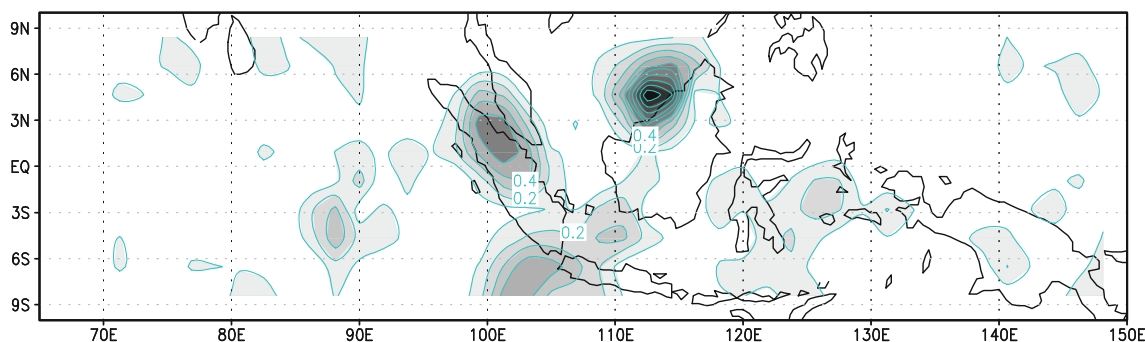


Fig. 19 Composite of the daily mean moisture convergence at 850 hPa difference between NO_DIURNAL and CTRL experiment at MJO phase 3 (contour interval is 0.2×10^{-6} g/kg/s)

and specific humidity and examine the results. Globally eliminating the diurnal cycle exerts a strong influence on the Maritime Continent. The mean state of precipitation increases and the intraseasonal variability becomes stronger over the region. Whereas the MJO is usually weakened when it passes over the Maritime Continent, it does maintain its strength in the NO_DIURNAL experiment. However, neglecting the diurnal signals during the integration does not change the propagating speed of the MJO.

As Inness and Slingo (2006) mentioned in their study, the enhanced diurnal cycle of convection may interfere with the relatively slow development of the MJO over the Maritime Continent by dissipating moist static energy on a

rapid time scale. We demonstrate that stronger MSE buildup occurs before the MJO convection develops over the Maritime Continent in NO_DIURNAL in comparison to MSE buildup in CTRL. The result suggests that deliberately diminishing the diurnal cycle in the model experiment consumes less MSE, leaving more MSE for the MJO’s buildup, an sufficient condition for the development of MJO convection in terms of the recharge–discharge theory of MJO. Along with the increased build up of MSE, composites of conditional instability and low-level moisture convergence provide supporting evidence for the amplification of the MJO in the experiment with a modulated diurnal cycle. With stronger moisture convergence

under the conditional instability, the MJO tends to maintain its amplitude by using enough MSE over the Maritime Continent in the NO_DIURNAL experiment.

While the present study attempts to concentrate on the impact of the diurnal cycle on the MJO, previous studies emphasized the direct influence of the topography in weakening the MJO as it passes over the Maritime Continent. Hsu and Lee (2005) focused on the relationship between MJO deep convection and tropical topography. They suggested that the lifting and frictional effects of the tropical topography and landmasses of the Maritime Continent under the prevailing surface easterly anomalies of the MJO induce the near-surface moisture convergence anomaly, which in turn triggers the deep heating anomaly. As a result, a subsequent new heating anomaly develops to the east of the topography. Meanwhile, the previous heating anomaly located to the west of the tropical topography weakens. Inness and Slingo (2006) investigated the blocking effect of the islands of the Maritime Continent using a simplified, aqua-planet version of GCM, with various idealized configurations of the Maritime Continent. They suggested the orography of the islands, rather than the presence of the islands themselves, as the main reason for the reduction in strength of the MJO as it passes over the Maritime Continent. Wu and Hsu (2009) addressed the blocking and wave-making effect of the topography on the MJO over the Maritime Continent. They found that the eastward movement of deep convection and near-surface wind anomalies in the MJO skirt the islands, resulting in a southward detour of the eastward-propagating MJO and a sudden shift of deep convection from one region to another. In addition, extra lifting and sinking within the large-scale circulation are induced by the topography, therefore modifying the behavior of the MJO in the Maritime Continent.

We do not rule out either the blocking effect of the islands or the influence of orography in the weakening of the MJO over the Maritime Continent. The existence of land–sea contrast over the region does trigger the diurnal cycle. However, the diurnal cycle itself may play a major role in controlling MJO intensity over the Maritime Continent. The continuing debate over theories regarding the MJO necessitates further investigation using high-resolution model with a more sophisticated land scheme.

Acknowledgments This work was funded by the Korea Meteorological Administration Research and Development Program under Grant CATER 2012-3061 (PN12010). We would like to thank the anonymous reviewers for their thoughtful comments and, especially Dr. Y. Ham, Dr. J. Lu, and Dr. S. Cocks for their helpful guidance.

References

- Back L, Bretherton C (2006) Geographic variability in the export of moist static energy and vertical motion profiles in the tropical Pacific. *Geophys Res Lett* 33:L17810. doi:10.1029/2006GL026672
- Bladé I, Hartmann D (1993) Tropical intraseasonal oscillations in a simple nonlinear model. *J Atmos Sci* 50:2922–2939
- Bloom S, Takacs L, Brin E (1996) Data assimilation using incremental analysis updates. *Mon Wea Rev* 124:1256–1271
- Bowman K, Collier J, North G, Wu Q, Ha E, Hardin J (2005) Diurnal cycle of tropical precipitation in Tropical Rainfall Measuring Mission (TRMM) satellite and ocean buoy rain gauge data. *J Geophys Res* 110
- Cane M, Molnar P (2001) Closing of the Indonesian seaway as a precursor to east African aridification around 3–4 million years ago. *Nature* 411:157–162
- Chen S, Houze R Jr (1997) Diurnal variation and life-cycle of deep convective systems over the tropical Pacific warm pool. *Q J R Meteorol Soc* 123(538):357–388
- Cocks S, LaRow T (2000) Seasonal prediction using a regional spectral model embedded within a coupled ocean atmosphere model. *Mon Wea Rev* 128:689–708
- Dayem K, Noone D, Molnar P (2007) Tropical western Pacific warm pool and maritime continent precipitation rates and their contrasting relationships with the Walker Circulation. *J Geophys Res* 112:D06101. doi:10.1029/2006JD007870
- Gill A (1980) Some simple solutions for heat induced tropical circulation. *Q J R Meteorol Soc* 106(449):447–462
- Hayashi Y (1979) Space-time spectral analysis of rotary vector series. *J Atmos Sci* 36:747–766
- Hendon H, Salby M (1994) The life cycle of the Madden-Julian oscillation. *J Atmos Sci* 51(15):2225
- Hsu H, Lee M (2005) Topographic effects on the eastward propagation and initiation of the Madden-Julian oscillation. *J Clim* 18:795–809
- Huffman G, Adler R, Arkin P, Chang A, Ferraro R, Gruber A, Janowiak J, McNab A, Rudolf B, Schneider U (1997) The global precipitation climatology project (GPCP) combined precipitation dataset. *Bull Am Meteorol Soc* 78(1):5–20
- Ichikawa H, Yasunari T (2006) Time-space characteristics of diurnal rainfall over Borneo and surrounding oceans as observed by TRMM-PR. *J Clim* 19:1238–1260
- Ichikawa H, Yasunari T (2008) Intraseasonal variability in diurnal rainfall over New Guinea and the surrounding oceans during Austral summer. *J Clim* 21(12):2852–2868
- Inness P, Slingo J (2006) The interaction of the Madden-Julian oscillation with the maritime continent in a GCM. *Q J R Meteorol Soc* 132(618):1645–1667
- Kemball-Cook S, Weare B (2001) The onset of convection in the Madden-Julian Oscillation. *J Clim* 14:780–793
- Kemball-Cook S, Wang B, Fu X (2002) Simulation of the intraseasonal oscillation in the ECHAM-4 model: the impact of coupling with an ocean model. *J Atmos Sci* 59:1433–1453
- Kikuchi K, Wang B (2008) Diurnal precipitation regimes in the global tropics*. *J Clim* 21:2680–2696
- Kim K, North G (1997) EOFs of harmonizable cyclostationary processes. *J Atmos Sci* 54:2416–2427
- Kim K, North G, Huang J (1996) EOFs of one-dimensional cyclostationary time series: computations, examples, and stochastic modeling. *J Atmos Sci* 53:1007–1017
- Kim D, Sperber K, Stern W, Waliser D, Kang I, Maloney E, Wang W, Weickmann K, Benedict J, Khairoutdinov M (2009) Application of MJO simulation diagnostics to climate models. *J Clim* 22(23):6413–6436
- Krishnamurti T, Low-Nam S, Pasch R (1983) Cumulus parameterization and rainfall rates II. *Mon Wea Rev* 111:815–828
- Krishnamurti T, Xue J, Bedi H, Ingles K, Oosterhof D (1991) Physical initialization for numerical weather prediction over the tropics. *Tellus* 43A:53–81

- Krishnamurti T, Rohaly G, Bedi H (1994) On the improvement of precipitation forecast skill from physical initialization. *Tellus* 46A:53–81
- Lee M, Schubert S, Suarez M, Bell T, Kim K (2007) Diurnal cycle of precipitation in the NASA Seasonal to Interannual Prediction Project atmospheric general circulation model. *J Geophys Res* 112:D16111. doi:[10.1029/2006JD008346](https://doi.org/10.1029/2006JD008346)
- Lim G, Suh A (2000) Diurnal and semidiurnal variations in the time series of 3-hourly assimilated precipitation by NASA GEOS-1. *J Clim* 13(16):2923–2940
- Madden R, Julian P (1994) Observations of the 40 50-day tropical oscillation a review. *Mon Wea Rev* 122(5):814–837
- Maloney D (2009) The moist static energy budget of a composite tropical intraseasonal oscillation in a climate model. *J Clim* 22:711–729
- Maloney E, Hartmann D (1998) Frictional moisture convergence in a composite life-cycle of the Madden–Julian oscillation. *J Clim* 11:2387–2403
- Mori S, Jun-Ichi H, Tauhid Y, Yamanaka M, Okamoto N, Murata F, Sakurai N, Hashiguchi H, Sribimawati T (2004) Diurnal land-sea rainfall peak migration over Sumatera Island, Indonesian maritime continent, observed by TRMM satellite and intensive rawinsonde soundings. *Mon Wea Rev* 132(8):2021–2039
- Neale R, Slingo J (2003) The maritime continent and its role in the global climate: a GCM study. *J Clim* 16(5):834–848
- Nunes A, Cocke S (2004) Implementing a physical initialization procedure in a regional spectral model: impact on the short-range rainfall forecasting over South America. *Tellus A* 56(2):125–140
- Oh J, Kim K, Lim G (2012) Impact of MJO on the diurnal cycle of rainfall over the western Maritime Continent in the austral summer. *Clim Dyn* 38:1167–1180
- Qian J (2008) Why precipitation is mostly concentrated over islands in the Maritime Continent. *J Atmos Sci* 65:1428–1441
- Rauniyar P, Walsh K (2011) Scale interaction of the diurnal cycle of rainfall over the Maritime Continent and Australia: influence of the MJO. *J Clim* 24:325–348
- Rodgers K, Latif M, Legutke S (2000) Sensitivity of equatorial Pacific and Indian Ocean water masses to the position of the Indonesian throughflow. *J Geophys Res* 18:2941–2944
- Rui H, Wang B (1990) Development characteristics and dynamic structure of tropical intraseasonal convection anomalies. *J Atmos Sci* 47(3):357–379
- Salby M, Hendon H (1994) Intraseasonal behavior of clouds, temperature, and motion in the Tropics. *J Atmos Sci* 51:2207–2224
- Sato T, Kimura F (2005) Diurnal Cycle of Convective Instability around the Central Mountains in Japan during the Warm Season. *J Atmos Sci* 62:1626–1636
- Seo K, Kim K (2003) Propagation and initiation mechanisms of the Madden-Julian oscillation. *J Geophys Res* 108(4384):10.1029
- Slingo J, Sperber K, Boyle J, Ceron J, Dix M, Dugas B, Ebisuzaki W, Fyfe J, Gregory D, Gueremy J (1996) Intraseasonal oscillations in 15 atmospheric general circulation models: results from an AMIP diagnostic subproject. *Clim Dyn* 12(5):325–357
- Slingo J, Inness P, Neale R, Woolnough S, Yang G (2003) Scale interactions on diurnal to seasonal timescales and their relevance to model systematic errors. *Ann Geophys* 46:139–155
- Sui C, Lau K, Takayabu Y, Short D (1997) Diurnal variations in tropical oceanic cumulus convection during TOGA COARE. *J Atmos Sci* 54:639–655
- Tian B, Waliser D E, Fetzner E J (2006) Modulation of the diurnal cycle of tropical deep convective clouds by the MJO. *J Geophys Res* 30:L20704. doi:[10.1029/2006GL027752](https://doi.org/10.1029/2006GL027752)
- Wheeler M, Hendon H (2004) An all-season real-time multivariate MJO index: development of an index for monitoring and prediction. *Mon Wea Rev* 132:1917–1932
- Wheeler M, Kiladis GN (1999) Convectively coupled equatorial waves: analysis of clouds and temperature in the wavenumber–frequency domain. *J Atmos Sci* 56:374–399
- Wu C, Hsu H (2009) Topographic Influence on the MJO in the Maritime Continent. *J Clim* 22:5433–5448
- Yang G, Slingo J (2001) The diurnal cycle in the tropics. *Mon Wea Rev* 129(4):784–801
- Yang S, Smith E (2006) Mechanisms for diurnal variability of global tropical rainfall observed from TRMM. *J Clim* 19:5190–5226
- Zhang C (2005) Madden-Julian Oscillation. *Rev Geophys* 43:RG2003. doi:[10.1029/2004RG000158](https://doi.org/10.1029/2004RG000158)